14th International Symposium on Turbulence and Shear Flow Phenomena (TSFP14)
Heidelberg, Germany, July 28–31, 2026

STATISTICAL MODELING OF THIRD-ORDER STRUCTURE FUNCTION IN WOVEN TURBULENCE WITH LUNDGREN SPIRAL VORTICES

Zhi Zheng
State Key Laboratory for Turbulence and Complex Systems
School of Mechanics and Engineering Science, Peking University
Beijing 100871, China
zhi.zheng@stu.pku.edu.cn

Yue Yang
State Key Laboratory for Turbulence and Complex Systems
School of Mechanics and Engineering Science, Peking University
Beijing 100871, China
yyg@pku.edu.cn

ABSTRACT

Building on the concept of "weaving turbulence", this study introduces woven Lundgren turbulence, a synthetic turbulence model constructed from Lundgren vortex ensembles. The turbulent field is assembled by distributing Lundgren spiral profiles along vortex filament centerlines, enabling control over stretching, temporal evolution, and spatial orientation. This approach integrates vortex stretching, spiral phase evolution, and viscous dissipation into a unified framework. Leveraging this construction, we derive an analytical expression for the third-order vorticity structure function in spectral space, which successfully recovers the K41 scaling law in the inertial range. Our analysis reveals that this K41 adherence arises from non-Gaussian vorticity correlations induced by the progressive stretching and tightening of spiral arms. Validation against direct numerical simulation at different Taylor-scale Reynolds numbers shows excellent agreement.

1 INTRODUCTION

Synthetic turbulence is a valuable tool for studying the fundamental mechanisms of turbulent flow. Two primary methodologies dominate this field. The first employs stochastic processes, such as fractal Lagrangian mapping on a random field, to generate velocity fields that mimic direct numerical simulation (DNS) data (Meneveau, 2011). The second, a more physically intuitive approach, generates turbulence by superimposing ensembles of elementary vortex structures (Pullin & Saffman, 1998). This vortex-based method links the dynamics of small-scale vortices to turbulence statistics, underscoring the importance of accurate vortex dynamic modeling.

Models for synthesizing turbulent vortices fall into three categories, each characterized by specific trade-offs. Stochastic methods offer computational speed by assembling random vortex elements, but lack a clear physical or dynamical basis (Dizaji *et al.*, 2018). Physics-based methods achieve high fidelity via directly simulating vortex dynamics, but are often computationally prohibitive (Aarnes *et al.*, 2025). Physics-informed generative models integrate machine learning with physical laws, yet remain dependent on training data and suffer from limited interpretability (Lozano-Durán & Bae, 2023).

Despite their differences, current models struggle to achieve multi-scale coupling within a unified framework. They are often scale-specific, performing well in either the inertial or dissipative range but failing to capture the transitions. For instance, vortex filament methods excel at modeling large-scale interactions, while analytical solutions like the Burgers and Lundgren vortices more accurately describe the internal evolution of small-scale dissipative structures. A unified model that integrates these complementary approaches is therefore necessary to bridge this gap, providing a complete physical picture across the entire energy spectrum.

Addressing this need, Shen *et al.* (2024) proposed "weaving turbulence", a technique for constructing entangled vortex tubes. The approach employs vortex filaments as centerlines to govern large-scale nonlinear dynamics, superimposing Burgers-like vortex profiles to establish a physical dissipation scale. Although this framework successfully reproduces the energy spectrum and second-order structure functions, it fails to capture odd-order statistics because axisymmetric Burgers vortices enforce Gaussian vorticity distributions with vanishing third-order moments. This statistical symmetry constraint necessitates a vortex model capable of generating inherent asymmetry to represent the skewness of turbulent fluctuations.

The Lundgren spiral vortex model (Lundgren, 1982) resolves this asymmetry deficit through unsteady differential rotation, which generates persistently skewed vorticity distributions via progressive spiral arm tightening. The Lundgren vortices naturally produce non-Gaussian correlations essential for third-order structure functions while encapsulating the essential features of fine-scale turbulence. Subsequent extensions to higher-order statistics (Pullin & Saffman, 1993; Saffman & Pullin, 1996) and scalar transport (Pullin & Lundgren, 2001) have confirmed the model's capacity to capture the non-Gaussian features required for energy transfer descriptions.

In this work, we propose woven Lundgren turbulence (WLT), which replaces the Burgers vortices in the weaving framework with Lundgren spiral vortices to explicitly incorporate unsteady stretching and spiral phase dynamics. To construct a physically consistent turbulent field, we distribute spiral vortices of varying evolutionary ages along entangled vortex-filament centerlines through a space-time mapping that couples arc-length coordinates to stretching history. Leveraging this construction, we derive an analytical expression for the third-order vorticity structure function in spectral space. It shows that the spiral tightening mechanism generates the requisite non-Gaussian correlations to recover the Kolmogorov scaling for the velocity structure function in the inertial range.

The paper is organized as follows. In §2, we describe the synthesis of turbulent fields using an adjustable spiral vortex ensemble based on weaving turbulence. In §3, we present a mathematical model for the third-order structure function in WLT, grounded in the statistical theory of the spiral vortex ensemble. The validation against DNS data at different Taylor-scale Reynolds numbers are shown in §4. Some conclusions are drawn in §5.

2 WEAVING TURBULENCE WITH LUNDGREN VORTICES

We construct woven turbulent fields comprising an ensemble of Lundgren vortices. This framework provides a platform for examining how vortex structures influence the third-order velocity structure function.

2.1 Lundgren Spiral Vortex Profiles

We adopt the methodology proposed by Lundgren (1993) to derive adjustable profiles for vortex tubes. The three-dimensional (3D) unsteady flow is represented as a two-dimensional (2D) unsteady spiral through a spatiotemporal stretching transformation, wherein the axial coordinate maps to time and the stretching compresses radial scales. The vorticity field of such a spiral vortex of age t is expressed through the real Fourier series

$$\omega(r,\theta,t) = \omega_0(r) + 2f(r)\times \sum_{n=1}^{\infty} \cos\left[2n(\theta-\mu(r)t)\right] \exp\left(-\frac{4n^2\mu'(r)^2\nu_L t^3}{3}\right), \tag{1}$$

where r and θ are the radial and azimuthal coordinates in the plane perpendicular to the vortex axis, $\omega_0(r)$ denotes the xisymmetric vorticity, $f(r)$ represents the amplitude of harmonics, $\mu(r)$ is the angular velocity profile, and ν_L is the viscous factor. The cosine term captures the $2n$-fold symmetric spiral arms rotating with $\mu(r)$, while the exponential factor accounts for viscous damping of fine-scale azimuthal structure. The progressive winding of these spiral arms arises from differential rotation, which is quantified by

$$\mu'(r) = \frac{\omega_0(r) - 2\mu(r)}{r}. \tag{2}$$

Note that $\mu'(r) \neq 0$ is a necessary condition for the spiral arms to tighten over time.

To obtain localized and smooth vorticity, we adopt the dimensionless radial profiles

$$\begin{aligned} \omega_0(r) &= \frac{\Gamma \exp\left[-(r/r_0)^2\right]}{(1+h)\pi r_0^2} + 2f(r), \\ f(r) &= \frac{\Gamma h (r/r_0)^2 \exp\left[-(r/r_0)^2\right]}{2(1+h)\pi r_0^2}, \end{aligned} \tag{3}$$

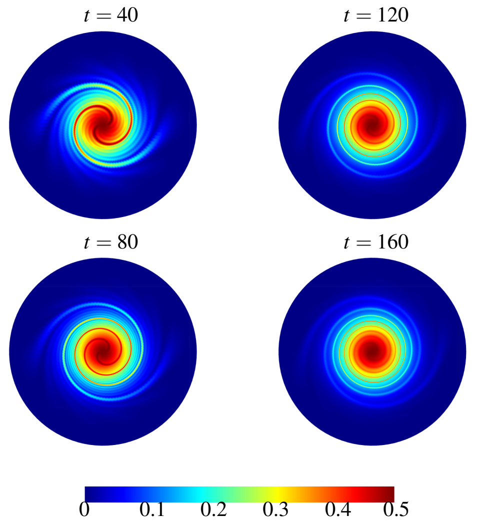

Figure 1. The vorticity of the spiral vortex profiles at different times t for dimensionless parameters $r_0 = 1$, $\Gamma = 1$, $\nu_L = 0.0001$ and $h = 0.5$.

where Γ represents the total circulation, r_0 denotes the vortex core radius, and h is a parameter governing the relative strength of the spiral arms.

Substituting Eq. (3) into Eq. (2), the angular velocity profile is

$$\mu(r) = \frac{\Gamma\left[1+h-\left(1+h+h(r/r_0)^2\right)\exp\left(-(r/r_0)^2\right)\right]}{2(1+h)\pi r_0^2}. \tag{4}$$

For $0 < h < 1$, Eq. (4) shows that $\mu(r)$ increases monotonically from zero at $r=0$ to a finite asymptotic value, while $f(r)$ peaks at a finite radius, thereby simulating the roll-up of vortex sheets.

Note that Eq. (1) introduces non-physical oscillations in the far-field, which result in localized singularities in the spiral arms and disrupt grid convergence. We retain the first ten dominant harmonics to preserve the essential dynamics of spiral tightening while ensuring smooth decay at large radii and convergence on computational grids. Figure 1 illustrates this temporal evolution, showing how the spiral arms constrict and increase in winding number as the vortex ages from $t = 40$ to 160. As time increases, one can see that two spiral arms persistently constrict, and the number of turns in the spiral increases due to differential rotation.

2.2 Constructing Lundgren Vortex Ensemble with Entangled Vortex Tubes

We consider an ensemble of Lundgren vortices randomly distributed in space, orientation, and age, following the original formulation of Lundgren (1982) and its extensions by Pullin & Saffman (1993). The ensemble is based on four fundamental assumptions: (i) ergodicity, which relates vorticity autocorrelators to velocity autocorrelators and is important in ensemble theory; (ii) locality of vorticity along each vortex axis, such that each vortex remains tube-like; (iii) random ages, orientations, and spatial positions of vortices, ensuring statistical homogeneity and isotropy; and (iv) a dynamical balance between vortex generation, stretching, and annihilation, which maintains a steady-state ensemble.

To construct a statistically stationary turbulent field, we distribute vortices of different evolutionary stages along spatial curves that serve as vortex centerlinee, as shown in Fig. 2. The central innovation of WLT lies in how we map the temporal evolution of Lundgren vortices onto these spatial curves, ensuring that the spatial distribution of vortex ages is physically consistent with the stretching history of the vortices themselves. The entangled vortex-filament skeletons of Shen *et al.* (2024) are employed, which provide a statistically stationary, homogeneous, and isotropic tangle of curves. Other techniques for weaving turbulence, including generating skeletons, constructing vorticity along curved centerlines, and boundary processing have been documented in previous studies (Xiong & Yang, 2019, 2020; Shen *et al.*, 2023, 2024).

The governing constraint arises from the physical requirement that a vortex element of age t, having been stretched with a constant strain rate γ_L, possesses an axial length $l(t) = l_0 e^{\gamma_L t}$, where l_0 denotes the initial length. Consequently, the arc-length coordinate s along the centerline must be related to t through

$$\frac{ds}{dt} = l_0 e^{\gamma_L t}. \tag{5}$$

To maintain statistical stationary, we consider a periodic life cycle for each closed centerline $\mathscr{C}$ of total arc length ℓ. A complete cycle consists of a growth phase from $t = 0$ to τ_L, followed by a decay phase where age decreases back to 0. The parameter τ_L represents the cutoff age of the vortices, denoting the stage at which the helical vortices in the ensemble undergo annihilation and subsequent reorganization. Integrating Eq. (5) over the growth phase yields the required arc length

$$\ell_{\text{up}} = \frac{l_0}{\gamma_L}(e^{\gamma_L \tau_L} - 1). \tag{6}$$

During the decay phase, the vortex tube at age $t = \tau_L - \tau$ retain length $l(\tau) = l_0 \mathrm{e}^{\gamma_L(\tau_L - \tau)}$, requiring an identical arc length $\ell_{\text{down}} = \ell_{\text{up}}$. Thus, a complete generation-to-annihilation cycle occupies a total arc length $\ell_{\text{cycle}} = \frac{2l_0}{\gamma_L}(\mathrm{e}^{\gamma_L \tau_L} - 1)$.

For a centerline of length ℓ, one accommodates $\mathscr{N} = \ell/\ell_{\text{cycle}}$ such cycles. $\mathscr{N}$ is assumed to be an integer for simplicity. This creates a periodic age profile that ensures continuous vortex regeneration along the filament.

For the growth phase $0 \le s \le \ell_{\text{up}}$,

$$t(s) = \frac{1}{\gamma_L} \ln\left(1 + \frac{\gamma_L s}{l_0}\right), \tag{7}$$

while for the decay phase $\ell_{\text{up}} \le s \le \ell_{\text{cycle}}$,

$$t(s) = \tau_L - \frac{1}{\gamma_L} \ln\left(1 + \frac{\gamma_L(s - \ell_{\text{up}})}{l_0}\right). \tag{8}$$

These functions are continuous and differentiable at $s = \ell_{\text{up}}$, satisfying $t(0) = 0$, $t(\ell_{\text{up}}) = \tau_L$, and $t(\ell_{\text{cycle}}) = 0$. This ensures smooth transitions between growth and decay. At any point s along a centerline, the local field is given by the Lundgren profile of Eq. (1). As one traverses the increasing branch, the structure evolves from a nascent, weakly wound spiral ($t = 0$) to a fully developed, tightly coiled state ($t = \tau_L$); traversing the decreasing branch, the spiral gradually unwinds and decays back to $t = 0$, completing the cycle. This construction ensures that the spatial distribution of ages along the centerline is consistent with the stretching history: vortex elements at different positions have physical lengths that exactly correspond to the arc-length increments over which they are distributed.

3 MODELLING THE THIRD-ORDER VELOCITY STRUCTURE FUNCTION IN WLT

We derive the third-order velocity structure function by evaluating the spectral density of vorticity correlations within the Lundgren ensemble. The WLT construction ensures statistical stationarity and homogeneity, permitting the replacement of ensemble averages with integrals over vortex age, orientation, and spatial position through the ergodicity assumption. The derivation proceeds through three sequential steps. First, we evaluate the third-order vorticity correlator $G^{\omega}(k)$ in spectral space by exploiting the localized geometry of the spiral arms. Second, we identify the inertial-range scaling behavior that connects vorticity correlations to velocity correlations. Third, we transform these spectral results to physical space to obtain the measurable structure function $D_3(r)$.

The evaluation of $G^{\omega}(k)$ relies on the Wentzel-Kramers-Brillouin-Jeffreys (WKBJ) approximation (Vallis, 2019). Applying this approximation to the ensemble of vortices distributed along the entangled filaments yields the spectral density

$$G^{\omega}(k) = \frac{1}{k} \frac{2\gamma_L \pi^2 N_c l_0}{L^3} \sum_{n=1}^{\infty} Z_n, \tag{9}$$

where

$$\begin{aligned} Z_n = -\sum_{m=-\infty}^{\infty} \int \frac{1}{\Omega'(u)^2 n} f_m(u) f_{n-m}(u) f_{-n}(u) \\ \times \exp\left[\frac{-2\nu_L (n^2 + m^2 + nm) k^2}{3\gamma_L n^2}\right] u du. \end{aligned} \tag{10}$$

Here, L denotes the domain size, N_c represents the number density of vortices, $\Omega(u)$ is the angular velocity of vorticity evolution in the stretched radial coordinate $u = S^{1/2} r_n(t)$. The factor $1/k$ arises from the Fourier transform of the localized spiral structure, while the exponential term accounts for viscous damping of the fine-scale azimuthal structure. The triple product $f_m f_{n-m} f_{-n}$ represents the nonlinear coupling between different spiral harmonics, resembling the triadic interactions governing energy transfer in turbulence (Kinjangi & Foti, 2023).

The exponential factor in Eq. (10) governs the dissipation-range behavior, where viscous effects smooth the finest spiral turns. Although the dissipation-range form is more complex than the Gaussian decay observed in second-order correlator Lundgren (1982), this complexity does not affect the inertial-range scaling law that constitutes the primary focus of our analysis. For any finite and non-zero f_n, Gaussian integrals yield a similar exponential cutoff factor, though it does not prevail within the relevant range of k. In our case, all $f_n(u)$ are equal (introduced in 2.1), so we could replace the sum over m by

$$\begin{aligned} I_n &= -\int_{-\infty}^{\infty} \exp\left[-\frac{2\nu_L(n^2 + m^2 + nm)k^2}{3\gamma n^2}\right] dm \\ &= -\exp\left(-\frac{2\nu_L k^2}{3\gamma n^2} \cdot \frac{3n^2}{4}\right) \int_{-\infty}^{\infty} \exp\left[-\frac{2\nu_L k^2}{3\gamma n^2}\left(m + \frac{n}{2}\right)^2\right] dm. \end{aligned} \tag{11}$$

For the inertial range, where $k \ll \sqrt{\frac{\gamma}{\nu_L}}$, the dissipation factor $\exp[-(\nu_L/2\gamma)k^2] \sim O(1)$. Therefore, the third-order vorticity

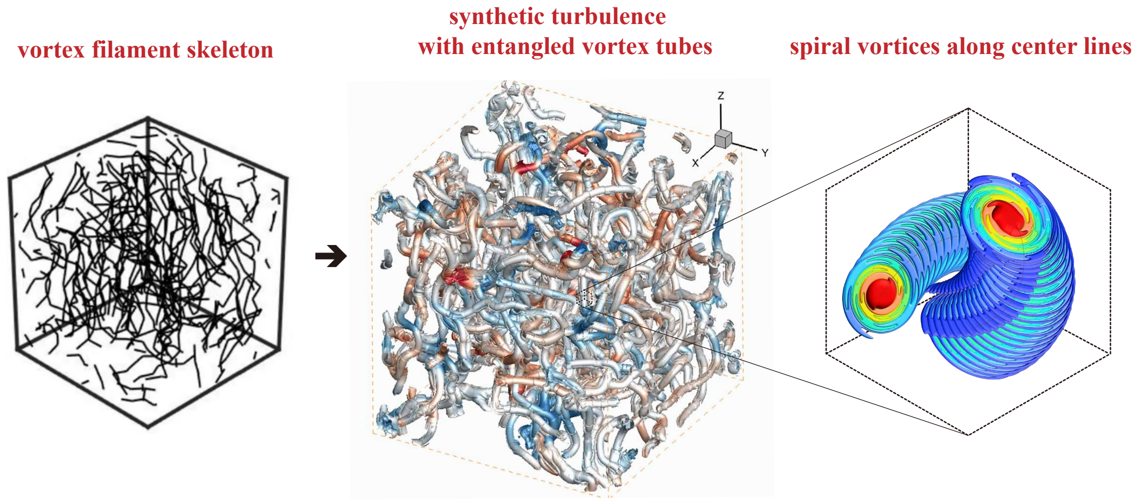

Figure 2. Schematic of Lundgren spiral vortex-based woven turbulence, where the turbulence field and vortex elements are colored by helicity density and vorticity strength, respectively.

correlation operator conforms $G^{\omega}(k) \sim k^{-1}$ within the inertial range. Through dimensional analysis $G(k) \sim G^{\omega}(k)/k^3$, the inertial-range scaling $G^{\omega}(k) \sim k^{-1}$ implies $G(k) \sim k^{-4}$.

Transforming from spectral space to physical space yields the measurable third-order velocity structure function. The structure function $D_3(r)$ relates to the velocity correlator $G(k)$ through the transformation (Saffman & Pullin, 1996)

$$\frac{D_3}{6} = 16\pi \int_0^{\infty} \left(\frac{\sin(kr)}{k^2r^2} + \frac{3\cos(kr)}{k^3r^3} - \frac{3\sin(kr)}{k^4r^4}\right)k^2 G(k)dk. \tag{12}$$

Substituting $G(k) = Bk^{-4}$ into Eq. (12) and changing variables to $y = kr$ yield

$$\frac{D_3}{6} = 16B\pi r \int_0^{\infty} \left(\frac{\sin(y)}{y^2} + \frac{3\cos(y)}{y^3} - \frac{3\sin(y)}{y^4}\right)y^{-2}dy. \tag{13}$$

Equation (13) establishes that $D_3(r) \sim r$ in the inertial range, consistent with the Kolmogorov scaling law (Kolmogorov, 1941). Incorporating the viscous correction, the third-order velocity structure function in WLT becomes

$$D_3(r) = K \cdot r \cdot \exp(\nu_L/2\gamma_L r^2), \tag{14}$$

where K is a constant to be fitted in different cases.

This result demonstrates that the non-Gaussian vorticity correlations are sufficient to recover the K41 scaling law without invoking additional phenomenological assumptions.

4 STATISTICS OF WLT

We simulated three cases with different Reynolds numbers, as summarized in Table 1. Figure 3 shows that the WLT model provides good agreement with both dissipation and enstrophy distributions, displaying the stretched-exponential shape for both.

To validate our theory, we compare the energy spectra and velocity structure functions against DNS data and the analytical model predictions, as shown in Fig. 4. The comparison shows good agreement. Discrepancies between the synthetic data, the analytical model, and the DNS results diminish as the Taylor-scale Reynolds number increases. Our analytical model accurately predicts the inertial-range scaling laws and the extent of the inertial range for the woven turbulence. Furthermore, the statistics of the synthetic field align well with the DNS results in the dissipative range.

Table 1. Three simulation cases with different Reynolds numbers of WLT, where k_t is Turbulent Kinetic Energy, $\langle\chi\rangle$ is Mean Enstrophy, $\langle\varepsilon\rangle$ is Mean Dissipation Rate, $\langle\nu_\lambda\rangle$ is Kinematic Viscosity, and Re_λ is Taylor Reynolds Number.

Group	k_t	$\langle\chi\rangle$	$\langle\varepsilon\rangle$	$\langle\nu_\lambda\rangle$	Re_λ
WLT1	3.95	7526.3	4.13	5.48×10^{-4}	231.3
WLT2	3.68	6488.2	3.89	5.99×10^{-4}	174.4
WLT3	3.02	5231.2	3.47	6.64×10^{-4}	131.6

We further evaluate the model by computing higher-order velocity structure functions for WLT and DNS data, benchmarking them against the K41 and SL-94 (She & Leveque, 1994) scaling laws, as shown in Fig. 5. The WLT shows excellent agreement with DNS for $p \leq 3$ and continues to track the classical K41 scaling closely for $p \leq 5$, only deviating slightly from the DNS statistics and SL-94 scaling. These results confirm that the realistic fine-scale vortical structures incorporated in WLT are essential for reproducing the fundamental statistics of turbulence.

5 CONCLUSIONS

We developed a synthetic turbulence field based on the Lundgren vortex ensemble model, capturing the key physics of vortex stretching and spiral evolution. Using this framework, we derived an analytical expression for the third-order structure function that recovers the K41 scaling law.

Our analysis reveals that the progressive stretching and tightening of spiral arms induces non-Gaussian spatial correlations in the vorticity field. This mechanism is pivotal for the third-order velocity structure function's adherence to the K41 scaling law and improves the predictive precision of higher-order statistics. Agreement with DNS data across a range of

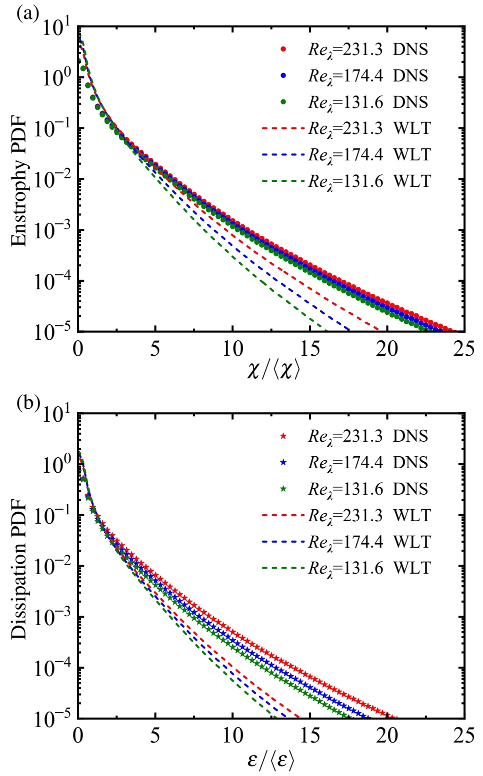

Figure 3. PDFs of enstrophy (a) and dissipation (b) normalized by their mean values for DNS and WLT at different Reynolds numbers.

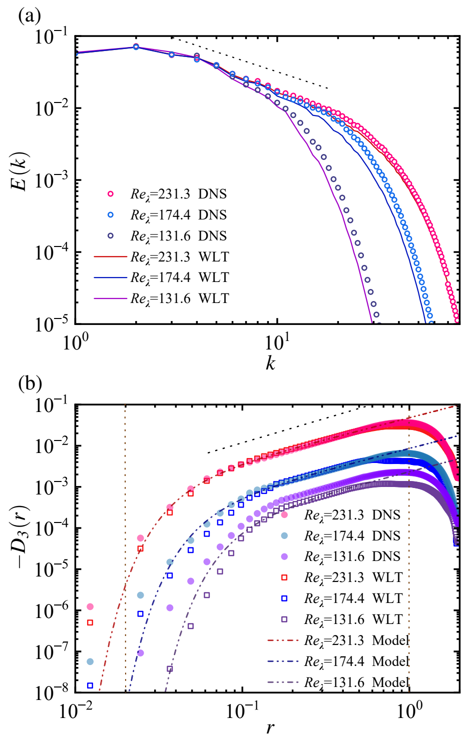

Figure 4. (a) Comparison of the energy spectra between DNS and the WLT at different Reynolds numbers. (b) Comparison of the third-order velocity structure functions among DNS, the WLT, and the theoretical model at different Reynolds numbers.

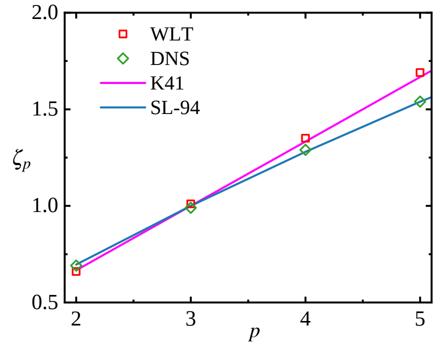

Figure 5. Scaling of the 2nd- to 5th-order velocity structure functions $D_p \sim r^{\zeta_p}$ for WLT and DNS, compared with the K41 and SL-94 predictions.

Reynolds numbers confirms the model's validity, demonstrating fidelity in both the inertial and dissipative ranges.

Future work will expand the framework to incorporate various vortex models, better representing the structural diversity of real turbulence.

APPENDIX: INVARIANTS OF THE VELOCITY GRADIENT TENSOR IN WLT

Considering the incompressible flows described by the 3D velocity field $u(x,t)$, the velocity gradient tensor (VGT) A or $A_{ij} = \partial u_i/\partial x_j$ effectively represents the local kinematics of fluid motion, capturing both the rate of deformation (strain rate) and rotation (vorticity) through the expression $A_{ij} = S_{ij} + \Omega_{ij}$. Here, $S_{ij} = (A_{ij} + A_{ji})/2$ denotes the symmetric strain-rate tensor, while $\Omega_{ij} = (A_{ij} - A_{ji})/2$ signifies the anti-symmetric rotation-rate tensor, related to the vorticity vector by $\omega_i = -\varepsilon_{ijk}\Omega_{jk}$. The first invariant $P = -\mathrm{tr}(A)$ vanishes identically due to the divergence-free condition $\partial u_i/\partial x_i = 0$ in incompressible turbulence, therefore we always use the second and third invariants

$$Q = -\frac{1}{2}A_{ij}A_{ji} = \frac{1}{4}\omega_i\omega_i - \frac{1}{2}S_{ij}S_{ij} \tag{15}$$

and

$$R = -\frac{1}{3}A_{ij}A_{jk}A_{ki} = -\frac{1}{3}S_{ij}S_{jk}S_{ki} - \frac{1}{4}\omega_i S_{ij}\omega_j \tag{16}$$

to analyze the local flow topology.

An important feature of the joint-PDF $P(Q,R)$ for the invariants Q and R is the tear-drop shaped contours. To facilitate comparisons across scales and Reynolds numbers, we adopt the normalized forms $Q^* = Q/\langle S_{ij}S_{ij}\rangle$ and $R^* = R/\langle S_{ij}S_{ij}\rangle^{3/2}$, based on the globally averaged strain-rate tensor $\langle S_{ij}S_{ij}\rangle$. Figure 6 compares the joint-PDF $P(Q^*,R^*)$ from DNS results with the WLT model. WLT reproduces, to great extent, the features observed in the DNS results, most notably the teardrop shape, which further validats its ability to capture the fine-scale topological features of turbulence.

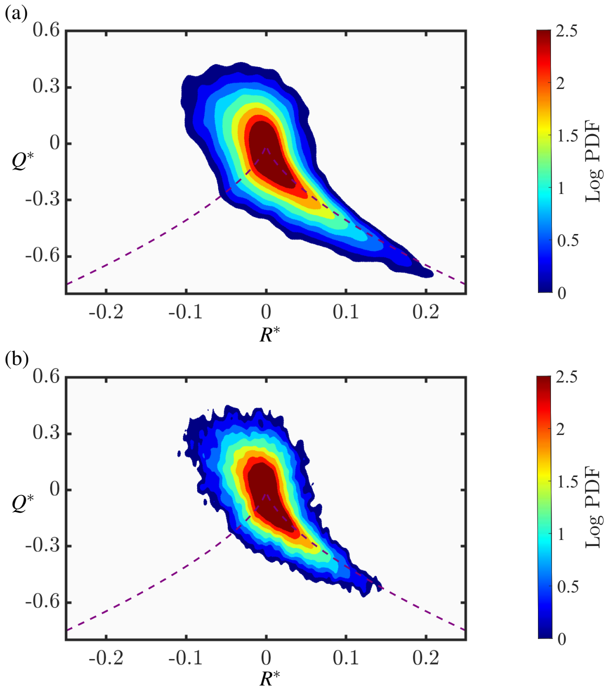

Figure 6. Logarithmically scaled joint-PDF for the normalized invariants Q^* and R^* in DNS (a) and WLT (b). --- denotes the Vieillefosse line (Vieillefosse, 1982, 1984).

REFERENCES

Aarnes, J. R., Babiker, O. M., Xuan, A., Shen, L. & Ellingsen, S. Å. 2025 "Vortex structures under dimples and scars in turbulent free-surface flows". *J. Fluid Mech.* **1007**, A38.

Dizaji, F. F., Marshall, J. S. & Grant, J. R. 2018 "A stochastic vortex structure method for interacting particles in turbulent shear flows". *Phys. Fluids* **30**, 013301.

Kinjangi, D. K. & Foti, D. 2023 "Characterization of energy transfer and triadic interactions of coherent structures in turbulent wakes". *J. Fluid Mech.* **971**, A7.

Kolmogorov, A. N. 1941 "The local structure of turbulence in incompressible viscous fluid for very large Reynolds numbers". *Dokl. Akad. Nauk SSSR* **30**, 299–303.

Lozano-Durán, A. & Bae, H. J. 2023 "Machine learning building-block-flow wall model for large-eddy simulation". *J. Fluid Mech.* **963**, A35.

Lundgren, T. S. 1982 "Strained spiral vortex model for turbulent fine structure". *Phys. Fluids* **25**, 2193.

Lundgren, T. S. 1993 "A small-scale turbulence model". *Phys. Fluids* **5**, 1472–1483.

Meneveau, C. 2011 "Lagrangian dynamics and models of the velocity gradient tensor in turbulent flows". *Annu. Rev. Fluid Mech.* **43**, 219–245.

Pullin, D. I. & Lundgren, T. S. 2001 "Axial motion and scalar transport in stretched spiral vortices". *Phys. Fluids* **13**, 2553–2563.

Pullin, D. I. & Saffman, P. G. 1993 "On the Lundgren-Townsend model of turbulent fine scales". *Phys. Fluids* **5**, 126–145.

Pullin, D. I. & Saffman, P. G. 1998 "Vortex dynamics in turbulence". *Annu. Rev. Fluid Mech.* **30**, 31–51.

Saffman, P. G. & Pullin, D. I. 1996 "Calculation of velocity structure functions for vortex models of isotropic turbulence". *Phys. Fluids* **8**, 3072–3084.

She, Z.-S. & Leveque, E. 1994 "Universal scaling laws in fully developed turbulence". *Phys. Rev. Lett.* **72**, 336–339.

Shen, W., Yao, J., Hussain, F. & Yang, Y. 2023 "Role of internal structures within a vortex in helicity dynamics". *J. Fluid Mech.* **970**, A26.

Shen, W., Yao, J. & Yang, Y. 2024 "Designing turbulence with entangled vortices". *Proc. Natl. Acad. Sci. U.S.A.* **121**, e2405351121.

Vallis, G. K. 2019 *Essentials of Atmospheric and Oceanic Dynamics*. Cambridge: Cambridge Univ. Press.

Vieillefosse, P. 1982 "Local interaction between vorticity and shear in a perfect incompressible fluid". *J. Phys.* **43** (6), 837–842.

Vieillefosse, P. 1984 "Internal motion of a small element of fluid in an inviscid flow". *Physica A* **125** (1), 150–162.

Xiong, S. & Yang, Y. 2019 "Construction of knotted vortex tubes with the writhe-dependent helicity". *Phys. Fluids* **31**, 047101.

Xiong, S. & Yang, Y. 2020 "Effects of twist on the evolution of knotted magnetic flux tubes". *J. Fluid Mech.* **895**, A28.